Large-Scale Simulations of Bubble-Induced Convection in a Liquid Layer

Eric Climent* and Jacques Magnaudet
Institut de Mécanique des Fluides de Toulouse, UMR CNRS-INPT-UPS 5502,
2 Avenue du Professeur Camille Soula, 31400 Toulouse, France
(Received 14 December 1998)

The flow pattern induced by a swarm of bubbles rising in a liquid layer is studied numerically. The fluid motion is described by spatially filtered Navier-Stokes equations forced by the presence of the bubbles. When the volume fraction and the residence time of the bubbles increase, a Rayleigh-Taylor-type instability develops. After transient stages, the flow reaches an equilibrium state made of counterrotating cellular structures. The simulations suggest that no wavelength selection mechanism exists in the present situation, making a striking difference with thermal convection. [S0031-9007(99)09346-1]

PACS numbers: 47.20.Bp, 47.55.Dz, 47.27.Te, 47.54.+r

Passive dispersion of bubbles, drops, and rigid particles in turbulent flows has received attention for a long time because of its paramount importance in many industrial and geophysical processes (see [1], for a recent review). It is only in recent years that situations in which the fluid motion is affected by the presence of the particles have begun to be considered. Most of the corresponding studies have focused on the modulation of turbulence [2,3] or on the distortion of vortices [4] produced by the interaction between the fluid and the dispersed phase. In these studies, because of the low volume fraction of particles which is generally considered, the effect of the particles on the underlying flow is rather small, while already significant. In contrast, there are physical situations in which the action of the particles may completely change the flow field or may even be the unique mechanism producing it, as in sedimentation problems. In this Letter we consider one of such situations, namely, the motions induced in a liquid layer of finite depth initially at rest by the rise of a large number of bubbles injected randomly.

To study this problem we use a numerical approach. Several levels of physical models are currently employed in the simulation of two-phase flows involving drops and bubbles. The most satisfactory from the conceptual point of view is certainly the direct numerical simulation approach in which all the scales of the flow, outside and inside the bubbles, are determined together with the shape of the interfaces by solving the exact Navier-Stokes equations which are assumed to be valid at the "microscopic" level. However, owing to the computer resources required by this approach, its practical applicability is currently limited to the study of problems involving a small number of bubbles [typically $O(10)$ to $O(10^2)$ [5]]. In the present case we intend to consider situations in which the number of bubbles is much larger, typically $O(10^4)$ to $O(10^5)$. Therefore we must turn to a different strategy involving some modeling of small-scale processes since it is no longer possible to solve the whole range of spatial scales present in the flow. To this end we have developed a large-scale simulation approach in which the Navier-Stokes equations are spatially filtered on "mesoscopic" control volumes V_f whose size λ is intermediate between the typical diameter of the bubbles d and the typical size of the large-scale structures of the flow $\mathcal{L}$. The essential result of this filtering procedure is to produce modified Navier-Stokes equations in which the effect of the bubbles on the flow appears through source terms. A detailed presentation of this model can be found in [6]. To lowest order in the volume fraction of the dispersed phase, the resulting equations governing the fluid motion are

$$\begin{cases} \nabla \cdot \langle \mathbf{u} \rangle = 0\,, \\ \rho_f \left[\frac{\partial \langle \mathbf{u} \rangle}{\partial t} + \langle \mathbf{u} \rangle \cdot \nabla \langle \mathbf{u} \rangle \right] = -\nabla \langle P \rangle \\ \quad + \nabla \cdot \left[\mu_E (\nabla \langle \mathbf{u} \rangle + {}^t \nabla \langle \mathbf{u} \rangle) \right] + \Phi_S\,, \end{cases} \tag{1}$$

in which $\langle \mathbf{u} \rangle$ and $\langle P \rangle$ denote the filtered velocity and pressure fields, with ρ_f being the density of the liquid and $\mu_E(\mathbf{x}, t)$ its effective viscosity which is generally different from its physical viscosity μ, as in a suspension. Here, this effective viscosity is introduced to take account of the small-scale dissipative effects associated to the wake of each bubble [7]. The source term $\Phi_S(\mathbf{x}, t)$ results from the momentum exchange between the two phases. Neglecting the density ρ_b of the bubbles compared to ρ_f, Φ_S can be written under the simple form

$$\Phi_S(\mathbf{x}, t) = \lim_{V_f \to 0} \frac{1}{V_f} \times \sum_{i=1}^{N_b} V_i \left[\rho_f \left(\frac{\partial \langle \mathbf{u} \rangle}{\partial t} + \langle \mathbf{u} \rangle \cdot \nabla \langle \mathbf{u} \rangle - \mathbf{g} \right) \right]. \tag{2}$$

In Eq. (2), V_i is the volume of bubble i and $\mathbf{g}$ denotes gravity, while $N_b(\mathbf{x})$ is the number of bubbles present at time t in the control volume $V_f(\mathbf{x})$. The quantity $\lim_{V_f \to 0} \sum_{i=1}^{N_b} V_i / V_f$ represents the volume fraction of bubbles at point $\mathbf{x}$ and time t. The source term Φ_S can be seen as a generalized buoyancy force which depends on the local volume fraction of bubbles. Consequently, in Eq. (1)

bubbles affect the liquid motion through an effective viscosity and through point forces. The spatial distribution of both quantities has to be found by determining at each time the position of each bubble. To this end we use a Lagrangian approach based on the following assumptions: (i) Surface tension forces are strong enough to maintain bubbles spherical; (ii) bubbles are free of any contamination so that the liquid can slip along the interfaces; (iii) coalescence and breakup phenomena occur so rarely that they can be neglected; (iv) bubble volume fractions do not exceed a few percent so that direct hydrodynamic interactions may be neglected (see, e.g., [8]); (v) pressure fluctuations in the flow have characteristic time scales much larger than the Rayleigh period of bubbles, so that no volume oscillation occurs; (vi) small-scale motions which are not predicted by Eq. (1), especially the potential flow due to the finite size of the bubbles and the rotational flow in their wake, do not affect bubble trajectories except through the coefficients involved in the expression of the various hydrodynamic forces. Under these assumptions, the position $\mathbf{x}^i(t)$ and the velocity $\mathbf{v}^i(t)$ of bubble i whose diameter is d_i are governed by

$$\begin{cases} \frac{d\mathbf{x}^i}{dt} = \mathbf{v}^i, \\ C_M \frac{d\mathbf{v}^i}{dt} = -\mathbf{g} + (1 + C_M)\left[\frac{\partial\langle\mathbf{u}\rangle}{\partial t} + \langle\mathbf{u}\rangle \cdot \nabla\langle\mathbf{u}\rangle\right] \\ \qquad\qquad -\frac{3}{4d_i} C_D(\mathrm{Re}_i)\,|\mathbf{v}^i - \langle\mathbf{u}\rangle|\,(\mathbf{v}^i - \langle\mathbf{u}\rangle) - C_L(\mathbf{v}^i - \langle\mathbf{u}\rangle) \times (\nabla \times \langle\mathbf{u}\rangle), \end{cases} \tag{3}$$

where $\mathrm{Re}_i = \rho_f|\mathbf{v}^i - \langle\mathbf{u}\rangle|d_i/\mu$ is the instantaneous value of the Reynolds number of bubble i. The second equation in (3) expresses the fact that the sum of the forces acting on each bubble is zero at any time since ρ_b/ρ_f is negligibly small. This equation is now recognized to allow a correct prediction of trajectories of isolated bubbles in slightly viscous flows. It takes into account the four most important hydrodynamic forces acting on a clean, spherical bubble of fixed radius, namely, buoyancy, added mass, viscous drag, and rotational lift. Recent analytical and numerical studies [9,10] have established the general expression of the added mass force and have demonstrated that the added mass coefficient C_M of a spherical particle is constant and equal to $\frac{1}{2}$ whatever the Reynolds number and the strength of the local acceleration. According to the results of direct simulations [10], the drag coefficient is taken to be $C_D(\mathrm{Re}_i) = 16(1 + 0.15\mathrm{Re}_i^{1/2})/\mathrm{Re}_i$ for $\mathrm{Re}_i \leq 50$, and $C_D(\mathrm{Re}_i) = 48(1 - 2.21\mathrm{Re}_i^{-1/2})/\mathrm{Re}_i$ [11] for $\mathrm{Re}_i \geq 50$. Finally it has been shown analytically [12] that $C_L = \frac{1}{2}$ in inviscid, weakly rotational, quasisteady flows. Direct numerical simulations [13] have revealed that for a bubble the variations of C_L are weak when Re_i is larger than unity, such that we use the above value whatever Re_i.

Equations (1)–(3) form a closed system as soon as boundary and initial conditions for $\langle\mathbf{u}\rangle$ and $\mathbf{v}^i$ are specified. The above model is now applied to a situation in which bubbles rise under the action of gravity in a layer of liquid of finite height initially at rest. Bubbles are injected randomly in time and space at the bottom of the layer and their initial velocity is chosen to be their rise velocity V_∞ in a liquid at rest. Bubbles then rise freely in the liquid until they reach the upper boundary, where they leave the computational domain as they would do at a free surface. All bubbles used in the present computations have the same diameter d_0, and their characteristic Reynolds number $\mathrm{Re}_\infty = \rho_f V_\infty d_0/\mu$ is about 4 (under usual conditions this corresponds to $d_0 \sim 0.2$ mm in water). Their average volume fraction $\overline{C}$ close to the injection is about 1%, so that assumption (iv) above is fairly well satisfied. Periodic conditions are imposed on the vertical boundaries $x = 0$ and $x = L$ while $\langle\mathbf{u}\rangle$ satisfies a no-slip (respectively, shear-free) condition on the lower (respectively, upper) boundary $y = 0$ (respectively, $y = H$). The aspect ratio L/H of the liquid layer is varied between $\frac{1}{2}$ and 4 ($d_0/L \sim 5 \times 10^{-4}$ in all cases), and we assume the large-scale motions determined by Eq. (1) to be two dimensional. The computational methods used to solve (1)–(3) are described in [6]; the computations corresponding to the figures below are performed on a 80×80 uniform grid.

Different flow regimes are observed, depending on $\overline{C}$ and on the characteristic residence time $T = H/V_\infty$. By an analogy with thermal convection to be discussed below, these regimes can be characterized by introducing a Rayleigh number defined as $\mathrm{Ra} = \rho_f g \overline{C} H^2/(\mu V_\infty)$ and a Prandtl number $\mathrm{Pr} = \mu/(\rho_f H V_\infty) = d_0/(H\mathrm{Re}_\infty)$. In the present computations the Prandtl number is set constant to the low value $\mathrm{Pr}_0 = 2.5 \times 10^{-4}$. When Ra is less than a critical value $\mathrm{Ra}_c(\mathrm{Pr}_0) \sim 2.0 \times 10^5$, the amplitude of the velocity fluctuations induced in the liquid remains much smaller than V_∞ and grows linearly with $\overline{C}$ in accordance with experimental results [14]. Consequently, bubbles rise almost in straight lines and no particular large-scale structure emerges when the flow field is averaged over times $O(T)$. The interesting feature of this regime is that the velocity fluctuations are highly anisotropic since we find that the vertical fluctuation is typically 2.8 times larger than the horizontal one. This anisotropy has been observed in many experiments, even if the value of the anisotropy ratio is still a subject of discussion.

A completely different regime occurs when Ra is increased beyond Ra_c. After an initial stage, the magnitude of the velocity fluctuations in the liquid becomes comparable to V_∞, making bubble trajectories significantly different from straight lines. Then at a given time $t < T$ (i.e., before the first bubbles reach the upper boundary), horizontal inhomogeneities related to the randomness of the injection begin to be amplified. Bubbles then accumulate quickly in mushroomlike regions producing intense upwelling motions (Fig. 1). The instability that develops

during this stage looks very similar to the usual Rayleigh-Taylor instability [15], since the mixture forming the lower part of the layer has a smaller density than the pure liquid located above. However, if several realizations of the flow are computed using the same set of control parameters, one observes that the horizontal spacing of the upwelling regions may vary by nearly 1 order of magnitude. This variation is obviously related to the distribution of the horizontal inhomogeneities of the injection which varies randomly from one realization to another. The sensitivity of the later stages of the instability to this initial condition suggests that in the present system no wavelength selection mechanism like the well-known effect of surface tension for immiscible liquids exists [15,16].

When time increases beyond T, Ra being still larger than Ra_c, the flow reaches a statistically steady state in which the rate of kinetic energy provided by the bubbles through the source term (2) is balanced by viscous dissipation. The flow is then made of a set of counterrotating cells and its structure looks at first glance very similar to the one observed in usual Rayleigh-Bénard convection. Bubbles fill the upwelling regions which drive the whole flow while very few bubbles stay in the downwelling zones (Figs. 2 and 3). The qualitative similarity between the plumes of bubbles observed here and the large "bubbly" regions free of particles occurring in fluidized beds when the gas velocity is increased beyond the fluidization limit [17] springs to mind. The maximum velocities in the liquid are comparable to or even larger than the rise velocity of the bubbles (they reach the value $4.4V_\infty$ in Fig. 3). Such stable cellular configurations are found up to $\mathrm{Ra} \sim 5.0\mathrm{Ra}_c$, the highest Rayleigh number for which computations have been carried out. It is highly tempting to make an analogy between the role of bubbles in the present problem and the role of hot fluid in thermal convection. Nevertheless, critical differences exist between the two phenomena as well as between their governing equations. First, the source term (2) differs from the usual buoyancy term because vertical density gradients cannot create any baroclinic torque in thermal convection while they can generate such a torque in the present situation since the fluid acceleration may have locally a significant horizontal component. Second, Eqs. (3) governing bubble motion differ strongly from the heat equation, especially because they do not involve any diffusion process (the Prandtl number introduced above must only be understood as the ratio between the residence time T of bubbles and the viscous diffusion time H^2/ν); however, in real flows second-order effects neglected in the present approach, like direct hydrodynamic interactions, may act as a random noise resulting in some diffusion. Last, owing to the absence of wavelength selection observed during the transient stage, the aspect ratio of the cells may vary greatly while it is known to remain close to unity in thermal convection [18]. Cells of various aspect ratios are easily observed in the computations (Figs. 2 and 3). We note similar tendencies in recently reported experiments [19]. In these experiments, hydrogen bubbles produced by means of electrolysis were released at

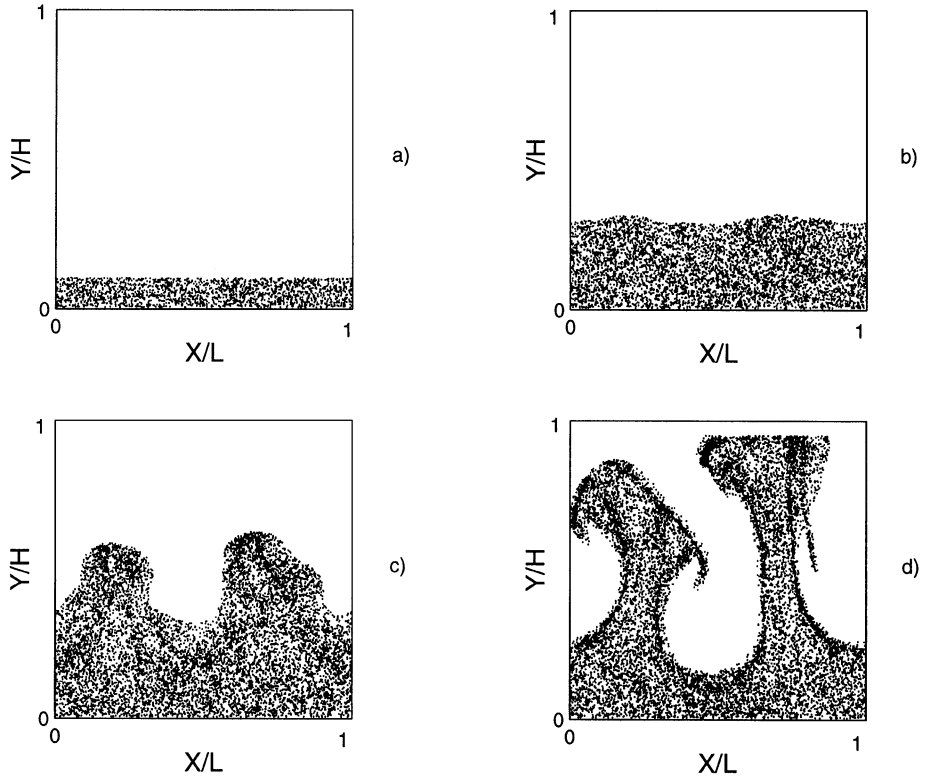

FIG. 1. Four stages of the development of the instability. $\mathrm{Ra} = 5.91 \times 10^5$; $L/H = 1$. (a) $t/T = 0.105$; (b) $t/T = 0.315$; (c) $t/T = 0.525$; (d) $t/T = 0.735$.

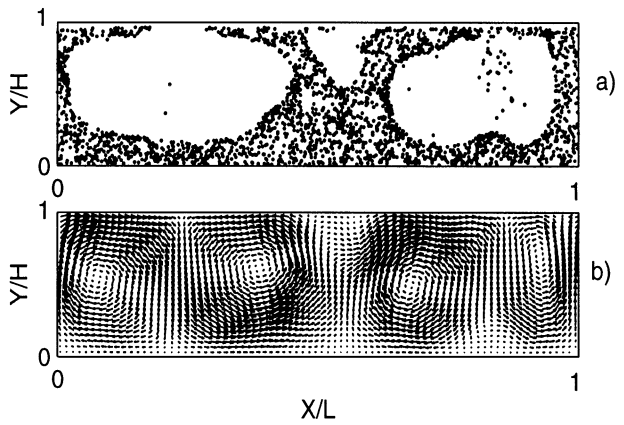

FIG. 2. Cells of aspect ratio 1 obtained for Ra $= 2.07 \times 10^5$ and $L/H = 4$. (a) Bubbles distribution; (b) velocity field.

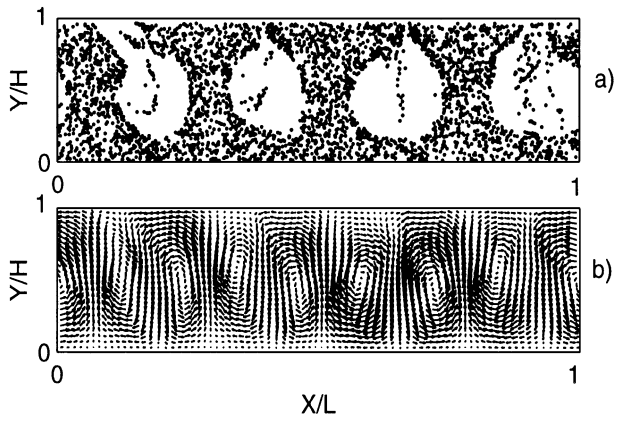

FIG. 3. Cells of aspect ratio $\frac{1}{2}$ obtained for Ra $= 2.07 \times 10^5$ and $L/H = 4$. (a) Bubbles distribution; (b) velocity field.

the bottom of a tank of water. The Rayleigh number was Ra $= 2.5 \times 10^5$, i.e., slightly above the threshold found in our computations, and the Prandtl number was higher (Pr $= 3.0 \times 10^{-2}$). The development and the characteristics of the instability reported by the authors for $t < T$ are very similar to those found in the present computations. In later stages they also observed a wide range of cell aspect ratios, from 0.9 to 0.1.

The present computations allow us to explore only two-dimensional flow patterns, so that it may well be that some phenomena which are crucial in the experiments, especially regarding the stability of the two-dimensional cellular pattern [20], are not captured here. Despite this limitation it appears that the model provided by Eqs. (1)–(3) is able to reproduce most of the observations carried out in the same range of parameters. This suggests that in that limited range the important phenomena are essentially two dimensional and that Eqs. (1)–(3) capture the large-scale physics of bubble-induced flows, at least in the dilute limit. We note that simulations based on lattice-gas methods and involving high concentrations of a mixture of "light" and "heavy" two-dimensional "bubbles" have already been reported [21]. In a certain range of parameters, the authors also observed the occurrence of large-scale circulations looking like Rayleigh-Bénard cells. As we have shown, bubble-induced convection is close but not similar to thermal convection. It provides a remarkable example of an inverse cascade process since the energy introduced at the small scale corresponding to the bubble diameter is finally transferred to large-scale cells. Three-dimensional computations are now needed to explore a wider range of parameters and to get a more complete view of the analogies and the differences existing between these two phenomena, especially regarding the nature of the successive bifurcations and the possible routes to turbulence. It is also highly desirable that carefully controlled laboratory experiments be performed as well, especially for specifying the limits of validity of mesoscopic models like the present one.

The computations reported in this Letter were carried out on the IBM-SP2 parallel computer of the "Centre National Universitaire Sud de Calcul" whose support is gratefully acknowledged.

*Present address: Institut de Mécanique des Fluides de Strasbourg, UMR CNRS-ULP 7507, 2 rue Boussingault, 67000 Strasbourg, France.

[1] J. C. R. Hunt, R. J. Perkins, and J. C. H. Fung, Appl. Mech. Rev. **47**, 50 (1994).
[2] K. D. Squires and J. K. Eaton, Phys. Fluids **2**, 1191 (1990).
[3] S. Elgobashi and G. C. Truesdell, Phys. Fluids **5**, 1790 (1993).
[4] G. R. Ruetsch and E. Meiburg, Phys. Fluids **6**, 2656 (1994).
[5] A. Esmaeeli and G. Tryggvason (to be published).
[6] E. Climent, Ph.D. thesis, Inst. Nat. Polytech. Toulouse, 1996.
[7] E. Climent and J. Magnaudet, C.R. Acad. Sci. Paris Ser. IIb **324**, 91 (1997).
[8] J. B. W. Kok, Eur. J. Mech. B, Fluids **12**, 515 (1993).
[9] T. R. Auton, J. C. R. Hunt, and M. Prud'Homme, J. Fluid Mech. **197**, 241 (1988).
[10] J. Magnaudet, M. Rivero, and J. Fabre, J. Fluid Mech. **284**, 97 (1995).
[11] D. W. Moore, J. Fluid Mech. **16**, 161 (1963).
[12] T. R. Auton, J. Fluid Mech. **183**, 199 (1987).
[13] D. Legendre and J. Magnaudet, J. Fluid Mech. **368**, 81 (1998).
[14] M. Lance and J. Bataille, J. Fluid Mech. **222**, 95 (1991).
[15] D. H. Sharp, Physica (Amsterdam) **12D**, 3 (1984).
[16] S. Chandrasekar, *Hydrodynamic and Hydromagnetic Stability* (Oxford University Press, Oxford, 1961).
[17] J. F. Davidson, D. Harrison, and J. R. F. Guedes de Carvalho, Annu. Rev. Fluid Mech. **9**, 55 (1977).
[18] C. Normand, Y. Pomeau, and M. Velarde, Rev. Mod. Phys. **49**, 581 (1977).
[19] R. Kimura and K. Iga, in *Mixing in Geophysical Flows*, edited by J. M. Redondo and O. Métais (CIMNE, Barcelona, 1995), pp. 35–51.
[20] R. Krisnamurti, J. Fluid Mech. **42**, 309 (1970).
[21] D. H. Rothman and L. P. Kadanoff, Comput. Phys. **8**, 199 (1994).